Journal of Materials Chemistry C

PAPER

Cite this: J. Mater. Chem. C, 2014, 2, 9934

Hollow nanocubes made of Ag–Au alloys for SERS detection with sensitivity of 10^{-8} M for melamine†

Ju-Mei Li,[ab] Yin Yang[ac] and Dong Qin*[a]

In this work, we transformed Ag nanocubes into Ag–Au hollow nanocubes with a continuous shell of Ag–Au alloy on the surface and some remaining pure Ag in the interior. Upon the removal of the pure Ag with aqueous H_2O_2 from inside of Ag–Au hollow nanocubes, we obtained Ag–Au nanoboxes. Next, we systematically evaluated the SERS properties of the hollow nanocubes and nanoboxes by benchmarking against the Ag nanocubes. In one study, we collected the SERS spectra of 1,4-benzenedithiol (1,4-BDT) adsorbed on the surfaces of the nanoparticles when the samples were prepared using 1,4-BDT solutions with different concentrations. Our results showed that both the hollow nanocubes and nanoboxes exhibited considerably stronger SERS activity than the original Ag nanocubes. In particular, the remaining pure Ag inside the hollow nanocubes made a significant contribution to achieve SERS detection with sensitivity of 10^{-11} M for 1,4-BDT. We further demonstrated their capability for the SERS detection of melamine at 10^{-8} M, a concentration considerably lower than the tolerance level of 1 ppm in infant formula. Moreover, we showed that the hollow nanocubes or nanoboxes with Ag–Au alloy shells on the surfaces were more stable compared to Ag nanocubes in an oxidative environment such as a solution containing an oxidant and/or halide ions. Taken together, these Ag–Au alloy nanostructures are good candidates for a trace detection of biological and chemical analytes by SERS.

Received 7th September 2014
Accepted 30th September 2014

DOI: 10.1039/c4tc02004a

www.rsc.org/MaterialsC

Introduction

Raman scattering spectroscopy can attain the "fingerprint" information of molecules from their vibrational transitions.[1] Despite all favorable aspects, the extremely small Raman scattering cross section, typically between 10^{-30} and 10^{-25} cm^2 per molecule,[2] makes it difficult to compete with laser-induced fluorescence spectroscopy (with a cross section on the order of 10^{-16} cm^2 per molecule) for trace detection.[3] Since the discovery by Van Duyne and Jeanmaire in 1977,[4] surface-enhanced Raman spectroscopy (SERS) has become as a powerful technique for the detection of molecules adsorbed on metal nanostructures with remarkably improved sensitivity. After several decades of exploration, it is now accepted that SERS relies on the localized surface plasmon resonance (LSPR) phenomenon and the enhancement of electromagnetic fields around a metal nanostructure to amplify the Raman scattering cross sections of molecules in proximity to the surface.[3] To this end, several groups have demonstrated that Ag and Au nanocrystals with sharp corners and edges could enhance the Raman scattering cross by 10^{10} or 10^{11} folds in terms of enhancement factor.[1,5] In addition, it was determined that the SERS activity of Ag nanocrystals was at least one order of magnitude higher compared to Au nanocrystals with a similar size and shape.[6] Accordingly, Ag-based SERS substrates have been widely explored for the trace detection of chemical and biological species.[7–11] Unfortunately, the susceptibility of Ag to oxidation often results in changes to the morphology, and thereby the deterioration of their SERS performance.

One strategy for improving the chemical stability of Ag nanocrystals without compromising the SERS activity is to form alloys with Au. In the past, several groups have investigated the SERS performance of Ag–Au alloy nanoparticles that were synthesized by the co-reduction of $HAuCl_4$ and $AgNO_3$ at different molar ratios.[12,13] Interestingly, Shin and coworkers showed that Ag–Au alloy nanoparticles with only 5% Ag content had SERS activity comparable to that of Ag nanoparticles.[14] Hwang and Brolo reported that the SERS activity of Ag–Au alloy nanoparticles was stronger than those for similar nanoparticles made of pure Ag or Au.[15] Additionally, they determined that the optimal composition of Ag in the alloy nanoparticles for achieving the strongest SERS activity had a dependence on the chemical nature of the probe molecule. While their results suggesting that the binding of a ligand to the alloy surface would affect SERS activity, there was no direct evidence to confirm the compositional homogeneity of Ag and Au across an alloy nanoparticle. As a result, it was difficult to understand the

[a]School of Materials Science and Engineering, Georgia Institute of Technology, Atlanta, Georgia 30332, USA. E-mail: dong.qin@mse.gatech.edu

[b]School of Materials Science and Engineering, Jingdezhen Ceramic Institute, Jingdezhen, Jiangxi 333403, P. R. China

[c]Department of Materials Science, Fudan University, Shanghai 200433, P. R. China

† Electronic supplementary information (ESI) available. See DOI: 10.1039/c4tc02004a

mechanisms behind the SERS enhancement. Most recently, Yin and co-workers demonstrated the formation of completely alloyed Ag–Au nanospheres by annealing Au–Ag core–shell nanospheres coated by SiO_2 at 930 °C.[16] They confirmed that the Ag–Au alloy nanospheres exhibited stronger SERS activity for detecting benzidine when compared with pure Ag or Au nanospheres, but they did not examine the detection sensitivity.

It has been well-established that the SERS activity of Ag nanocubes with sharp corners and edges is 25 fold stronger compared to that of Ag nanoshperes.[17] In principle, one can deposit a thin shell of Ag–Au alloy on the outmost surface of Ag nanocubes to obtain excellent SERS performance, together with considerably improved chemical stability. In the past years, the galvanic replacement reaction between Ag nanocubes and $HAuCl_4$ has been extensively used to generate hollow nanocages made of Ag–Au alloys.[18] Unfortunately, the production of one Au atom at the expense of three Ag atoms from Ag nanocubes results in a significant loss of Ag, leading to the deterioration of SERS activity.[19] One possible solution to mitigate the loss of Ag element is to introduce another chemical reducing agent to complement the galvanic replacement reaction. Mirkin,[20] Lizmarzan,[21] and Xue[22] were among the first to demonstrate that the reduction of the Ag^+ ions originating from the galvanic replacement reaction by ascorbic acid (AA) could generate Ag atoms for their co-deposition with Au atoms onto the Ag nanoplates for the formation of Ag–Au alloy nanoplates. Most recently, we further extended their methodology to transform Ag nanocubes into Ag–Au hollow nanostructures with 80% Ag retained in their walls and interiors.[23]

In this work, we used our previously reported protocol[23] to produce Ag–Au alloy hollow nanocubes and Ag–Au alloy nanoboxes for a systematic evaluation of their sensitivity for SERS detection. Previously, we only compared the SERS properties of Ag–Au hollow nanocubes at two different excitation wavelengths of 532 and 785 nm, together with a discussion on the role of Ag enrichment in increasing their SERS activity.[23] However, we were unable to systematically assess the detection sensitivity of this new class of Ag–Au nanostructures using different types of SERS probe molecules. Herein, we developed a procedure for functionalizing the Ag–Au alloy nanostructures with three types of probe molecules, including 1,4-benzenedithiol (1,4-BDT), 4-aminobenzenethiol (4-ABT), and melamine, without forming aggregation. We confirmed the adequacy of this procedure by collecting UV-vis spectra from the suspensions before and after the nanostructures had been functionalized with the probe molecule at different concentrations. Only when there was essentially no change to the UV-vis spectra, we would proceed to collect the SERS spectra at an excitation wavelength of 785 nm. When 1,4-BDT was used, we determined that the Ag–Au hollow nanocubes exhibited the strongest SERS activity, with a detection limit as low as 10^{-11} M. We further demonstrated a SERS detection limit of 10^{-8} M for melamine, which is well below the tolerance level of 1 ppm in infant formula. Our results suggest that both the remaining pure Ag inside the hollow nanocubes and the Ag–Au alloy shells on the surfaces could contribute to the significantly enhanced SERS performance of the Ag–Au hollow nanocubes. Finally, the Ag–Au alloy shell on the surface of the hollow nanocubes could significantly improve their stability in phosphate buffer, NaCl, and H_2O_2 aqueous solutions.

Experimental section

Preparation of Ag nanocubes

The Ag nanocubes were synthesized using ethylene glycol (EG, J. T. Baker, lot no. G32B27) as a solvent and silver trifluoroacetate (CF_3COOAg, Aldrich) as a precursor of elemental silver. In a typical experiment, EG (5 mL) was added into a round bottom flask (100 mL, ACE Glass) and heated under magnetic stirring in an oil bath at 150 °C, followed by the fast injection of NaHS (0.06 mL, 3 mM in EG, Aldrich, 02326AH). After 2 min, HCl (0.5 mL, 3 mM in EG, Aldrich) and poly(vinylpyrrolidone) (PVP-55, MW ≈ 55 000, 1.25 mL, 20 mg mL^{-1} in EG, Aldrich) were sequentially added. After another 2 min, CF_3COOAg (0.4 mL, 282 mM in EG) was introduced. During the entire process, the flask was capped with a glass stopper except for the addition of reagents. Once the major LSPR peak of the Ag nanocubes had been tuned to 435 nm, the reaction was quenched in an ice-water bath. Upon centrifugation and washing with acetone and deionized (DI) water three times, the nanocubes were re-dispersed in DI water for future use.

Synthesis of Ag–Au hollow nanocubes and nanoboxes

In a typical synthesis, 2 mL of PVP-29 (MW ≈ 29 000, 29 mg mL^{-1}) aqueous solution was injected into a 23 mL glass vial, followed by the introduction of 0.5 mL of aqueous ascorbic acid (100 mM) and 9 μL Ag nanocubes (7.47×10^{10} particles in all) under magnetic stirring. Next, 0.6 mL of aqueous $HAuCl_4$ (0.2 mM) was titrated into the reaction solution at a rate of 0.02 mL min^{-1} using a syringe pump. After the titration was completed in 35 min, the resultant Ag–Au hollow nanocubes were collected by centrifugation at 10 000 rpm for 15 min, washed with DI water three times, and stored in DI water. The Ag–Au nanoboxes were generated by mixing 5 mL of the as-obtained Au–Ag hollow nanocubes with 5 mL of 2% H_2O_2 for 12 h. The resultant Ag–Au nanoboxes were washed twice with DI water and re-dispersed in 5 mL of DI water. The particle concentrations of the Ag–Au hollow nanocubes and Ag–Au nanoboxes were derived from the particle concentration of the original Ag nanocubes prior to reaction, with an assumption that each nanocube would generate one Ag–Au hollow nanocube or nanobox with no loss in terms of number of particles during the washing steps.

Instrumentation and characterization

The UV-vis-NIR spectra were collected using a Cary 50 spectrometer (Agilent Technologies, Santa Clara, CA). Dynamic light scattering (DLS) characterization was conducted with a Nano ZS Zetasizer (model ZEN3600, Malvern Instruments) using a He–Ne laser with a wavelength of 632.8 nm. Transmission electron microscopy (TEM) images were taken using a Hitachi HT7700 microscope (Hitachi, Tokyo, Japan) operated at 120 kV. The elemental measurements of Au and Ag were performed using an inductively coupled plasma mass spectrometer (ICP-MS,

NexION 300Q, PerkinElmer, Waltham, MA). A conventional centrifuge (Eppendorf 5430) was used for the collection and washing of all the samples.

Surface-enhanced Raman spectroscopy measurements

The as-prepared nanoparticles were collected by centrifugation at 8000 rpm for 15 min, washed once with DI water, collected again by centrifugation at 7000 rpm for 15 min, and finally dispersed in 1 mL of 1,4-BDT or 4-ABT solutions in ethanol at different concentrations for 1 h. For melamine, the nanoparticles were incubated in aqueous solutions of melamine with various concentrations for 4 h. The functionalized nanoparticles were collected by centrifugation at 6000 rpm for 15 min, washed with DI water once, collected again by centrifugation at 7000 rpm for 15 min, and then dispersed in 1 mL of DI water for UV-vis measurement. We always confirmed that there was no change to the UV-vis spectra of the nanoparticles before and after they had been functionalized with the probe molecule, and then proceeded to conduct SERS measurements. We maintained a concentration of 2.4×10^{10} particles per mL for all the samples.

We attached a polydimethylsiloxane (PDMS) block to a glass slide for fabricating a sample cell. A small hole was punched in PDMS in advance to hold 20 μL of liquid sample. A glass cover slip with a thickness of 170 μm was placed on the top to prevent solvent evaporation. It also served as a reference point, from which the focal plane was lowered to 200 μm into the sample. We used an excitation source of 785 nm at a power of 50 mW. The Raman spectra were collected from the solution phase using a Renishaw inVia Raman spectrometer coupled with a Leica microscope with a 100× objective lens and a holographic notch filter with a grating of 1200 lines per mm. We started each SERS measurement by recording the spectra with a collection time of 1 s. Only when the SERS signals were stable, indicating the absence of aggregation in the aqueous suspension, we would further improve the signal to noise ratio by increasing the collection time to 30 and 150 s for 1,4-BDT (or ABT) and melamine, respectively.

Results and discussion

Formation of Ag–Au hollow nanocubes and nanoboxes

Fig. 1 outlines the transformation of Ag nanocubes into Ag–Au hollow nanocubes and nanoboxes in an aqueous solution containing poly (vinyl pyrrolidone) (PVP) (a stabilizing agent) and AA (a reducing agent), followed by the titration of $HAuCl_4$ aqueous solution using a syringe pump at room temperature. The galvanic replacement reaction between Ag nanocubes and $HAuCl_4$ resulted in the dissolution of Ag atoms from the interior of Ag nanocubes by oxidation into Ag^+ ions. Concurrently, the co-reduction of $AuCl_4^-$ ions and the Ag^+ ions by AA led to the generation of Ag and Au atoms for their co-deposition onto the surface of the Ag nanocubes. As a result, Ag nanocubes were transformed into Ag–Au hollow nanocubes with few Ag remaining in the interiors. Upon the removal of the residual Ag with aqueous H_2O_2, Ag–Au nanoboxes were formed.

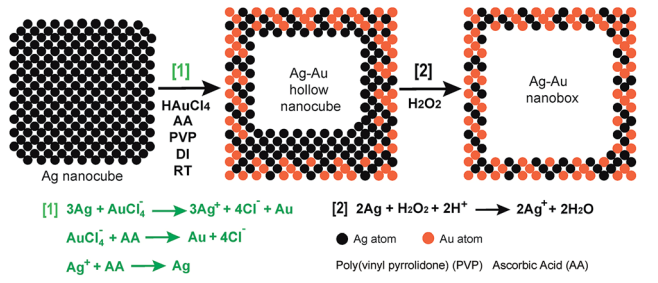

Fig. 1 Schematic illustration for the transformation of a Ag nanocube into a Ag–Au hollow nanocube and a Ag–Au nanobox.

Fig. 2A displays a transmission electron microscopy (TEM) image of the Ag nanocubes with an edge length of around 39.2 nm. As demonstrated in our previous work, we could easily maneuver the morphology and composition of the Ag–Au hollow nanocubes by changing the amount of $HAuCl_4$ added into the aqueous suspension of Ag nanocubes in the presence of AA.[23] For example, with the addition of 0.6 mL $HAuCl_4$ (0.2 mM), we obtained Ag–Au hollow nanocubes with an edge length of about 50.5 nm, as shown in Fig. 2B. With an increase in the average edge length from 39.2 to 50.5 nm for the nanocubes, we estimated a thickness of 5.6 nm for the Ag–Au alloy shell. The Ag–Au hollow nanocubes possessed sharper corners and edges because of the preferential deposition of Au and Ag atoms at the edges and corners.[24] On the basis of inductively coupled plasma mass spectrometry (ICP-MS), the Ag–Au hollow nanocubes presented 80% Ag content and a Au to Ag molar ratio of 1 : 5.2. Upon removing Ag with 2% aqueous H_2O_2, we generated Ag–Au nanoboxes with a continuous Ag–Au shell, as indicated by the

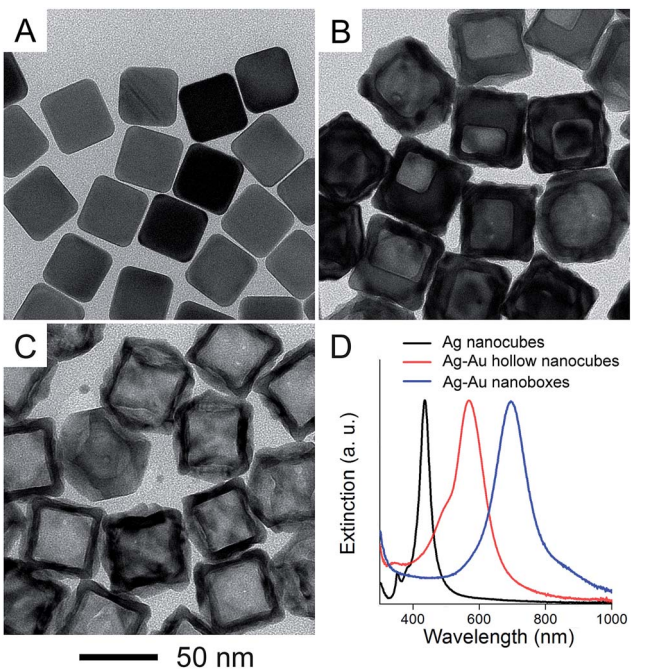

Fig. 2 TEM images of (A) Ag nanocubes; (B) Ag–Au hollow nanocubes; and (C) Ag–Au nanoboxes. (D) UV-vis-NIR spectra of the samples shown in (A–C).

TEM image in Fig. 2C. As confirmed by ICP-MS measurement, the Ag–Au nanoboxes were made of Ag–Au alloy with a Au to Ag molar ratio of 1 : 1.7.

We monitored the transformation of Ag nanocubes into Ag–Au hollow nanocubes, and then nanoboxes by UV-vis-NIR spectroscopy. As shown in Fig. 2D, the LSPR peak of the Ag nanocubes was shifted from 435 to 572 nm, together with the broadening in peak width and the appearance of a shoulder peak at 502 nm for the formation of Ag–Au hollow nanocubes. Upon removing the residual Ag in the interiors, the LSPR peak of the Ag–Au hollow nanocubes was further shifted from 572 to 699 nm, indicating the formation of Ag–Au nanoboxes. We also demonstrated the capability to reproducibly obtain identical batches of Ag–Au hollow nanocubes by introducing a specific amount of aqueous $HAuCl_4$ into the suspensions of Ag nanocubes to tune their LSPR peaks to 572 nm. As shown in Fig. S1,† the UV-vis spectra of the Ag–Au hollow nanocubes essentially showed no changes after they had been stored in DI water for up to 180 days, indicating good stability for the nanoparticles.

SERS characterization of the Ag–Au hollow nanocubes and nanoboxes

We evaluated the SERS performance of the Ag–Au hollow nanocubes and nanoboxes by benchmarking against the Ag nanocubes. Significantly, we used a protocol to functionalize the nanoparticles with a SERS probe without forming aggregates (see details in the Experimental section). We collected UV-vis spectra and dynamic light scattering data from the suspension of nanoparticles before and after they had been functionalized to ensure the absence of aggregates. As shown in Fig. S2 and S3,† there were essentially no changes to the UV-vis spectra and the hydrodynamic size distribution of the Ag–Au hollow nanocubes before and after they had been functionalized with 1,4-BDT (10^{-11} M) and melamine (10^{-8} M). We fixed the concentration at 2.4×10^{10} particles per mL for all SERS measurements. Fig. 3A–C, shows the SERS spectra of 1,4-BDT enhanced with the Ag nanocubes, Ag–Au hollow nanocubes, and Ag–Au nanoboxes, respectively, when the concentration of 1,4-BDT was in the range from 10^{-8} to 10^{-11} M. The SERS peaks located at 1063, 1178 and 1563 cm^{-1} are associated with the C–S stretch (ν_{7a}), C–H bend (ν_{9a}), and C–C stretch (ν_{8a}) modes,[19] respectively. Based on the SERS peak intensity at 1563 cm^{-1}, we found that the SERS detection sensitivity of 1,4-BDT was confirmed to be 10^{-11} and 10^{-10} M for Ag–Au hollow nanocubes and nanoboxes, respectively. In comparison, there was no discernible SERS peak for Ag nanocubes when the concentration of 1,4-BDT was decreased to 10^{-10} M. The strongest SERS signals for the Ag–Au hollow nanocubes suggest that the continuous shells of Ag–Au alloy on the surfaces of hollow nanocubes might play an important role, which is consistent with previous work.[16] Moreover, the sharpened corners and edges of the Ag–Au hollow nanocubes could serve as hot spots with dramatic enhancement in the local electric field. Upon the removal of the residual Ag in the interiors of the Ag–Au hollow nanocubes, the SERS activity of the Ag–Au nanoboxes decreased. This observation suggests that the inclusion of pure Ag in the interior could drastically increase the SERS activity. On the other hand, the Ag–Au nanoboxes showed stronger SERS activity over the Ag nanocubes, suggesting that the Ag–Au shell of 5.6 nm thickness also played an important role in enhancing the local electric field.

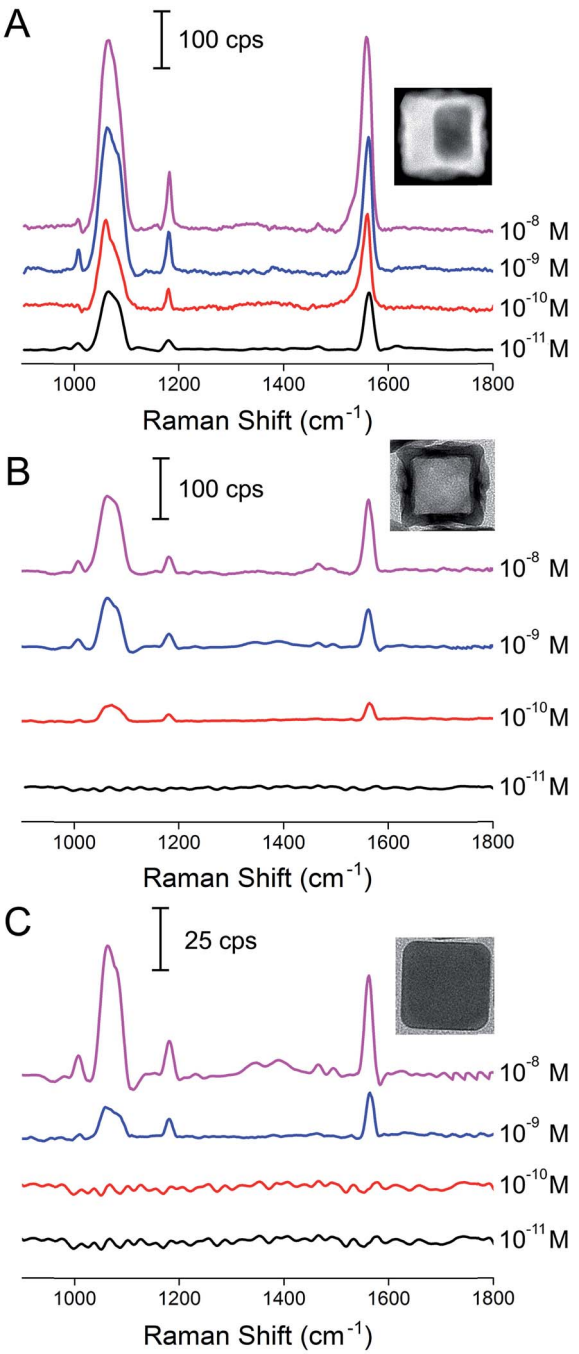

Fig. 3 SERS spectra of 1,4-BDT adsorbed on the surfaces of (A) Ag–Au hollow nanocubes, (B) Ag–Au nanoboxes, and (C) Ag nanocubes when 1,4-BDT solutions with different concentrations were used to functionalize the nanoparticles. The insets of A–C are TEM images of Ag–Au hollow nanocubes, Ag–Au nanoboxes, and Ag nanocubes, respectively.

On the basis of a reported protocol,[19] we used the strongest SERS peak at 1563 cm^{-1} to calculate the SERS enhancement factor (EF). We assumed that a complete monolayer of 1,4-BDT molecules with a footprint of 0.54 nm^2 covered the surface of the nanostructures. As a result, the calculated value corresponds to a theoretical maximum number of molecules and thereby the EF reported here should be an underestimate of the actual value. Using the particle size measured by TEM, we estimated the surface area of a Ag nanocube and a Ag–Au hollow nanocube to be 9.2×10^3 nm^2 and 1.5×10^4 nm^2, respectively. Hence, the EF values were calculated to be 3.1×10^5, 4.6×10^6 and 1.0×10^7 for the Ag nanocubes, Ag–Au nanoboxes, and Ag–Au hollow nanocubes, respectively.

To further elucidate the feasibility of SERS detecting the binding of different probe molecules, we collected SERS spectra from 1,4-BDT and 4-ABT adsorbed on the surfaces of the Ag–Au hollow nanocubes when the samples were prepared with 1,4-BDT or ABT solution at a concentration of 10^{-9} M. As shown in Fig. 4, we clearly observed three major peaks that can be assigned to the vibration modes of ν_{7a}, ν_{9a}, and ν_{8a} for these two molecules. When compared with their Raman shifts, we noticed that the C–S stretch (ν_{7a}) and C–C stretch (ν_{8a}) modes of 4-ABT were blue shifted from 1077 to 1090 cm^{-1} and 1563 to 1588 cm^{-1}, respectively. On the other hand, there was essentially no change for the C–H bend mode. We also collected the Raman spectra from solid samples of 1,4-ABT and 4-BDT (Fig. S4†), their C–C stretch (ν_{8a}) modes were positioned at 1577 cm^{-1} and 1596 cm^{-1}, respectively. As a result, when 1,4-BDT and 4-ABT bind to the surfaces of the Ag–Au hollow nanocubes, their ν_{8a} modes were changed from 1577 to 1563 cm^{-1} and 1596 to 1588 cm^{-1}, respectively. The smaller difference in Raman shift (8 cm^{-1}) for 4-ABT indicates weaker binding to the surface of the Ag–Au hollow nanocubes.

SERS detection of melamine

Melamine (1,3,5-triazine-2,4,6-triamine, $C_3H_6N_6$) is an organic compound that has been extensively applied to produce melamine–formaldehyde resins. Over the past few years, a high melamine level has been discovered in eggs, wheat gluten, and various milk products. While melamine is not a toxic chemical, the combination of melamine with cyanuric acid may form insoluble crystals in kidneys; thus, leading to kidney malfunction in humans and even death in babies. At present, the safety limits of melamine are 1 and 2.5 ppm for the infant formula in China and the United States, respectively.[25] Recently, SERS has been extensively developed for the rapid and label-free detection of melamine.[26–28] In most of the previous studies, Ag and Au nanoparticles have been used as the SERS substrates to measure the amount of melamine adsorbed on the surfaces, but the detection sensitivity has been limited to 10^{-7} M, together with challenges in reproducibility because of the aggregation of nanoparticles.[29]

Here, we used the Ag–Au hollow nanocubes to detect the trace amount of melamine in an aqueous solution. In a typical experiment, we mixed the Ag–Au hollow nanocubes with aqueous melamine solutions with various concentrations for 4 h. Then, we centrifuged down the nanoparticles, decanted the supernatant, washed the particles with DI water twice, and finally re-dispersed the melamine-derivatized hollow nanocubes in DI water for SERS measurement (the nanoparticle concentration is 2.4×10^{10} particles per mL). Fig. 5 shows the SERS spectra of melamine with concentrations in range of 10^{-5} to 10^{-8} M. The peak at 701 cm^{-1} can be assigned to the triazine deformation band of melanine.[25] We could clearly resolve this peak at a concentration of 10^{-8} M according to the SERS spectra, which is well below the tolerance level of 1 ppm in infant formula. To demonstrate the feasibility of SERS detection using a real sample, we performed melamine detection in liquid milk. As shown in Fig. S5,† we were still able to observe the characteristic peak of melamine at a concentration of 10^{-8} M in liquid milk.

Stability test of the Ag–Au hollow nanocubes and nanoboxes

The deposition of Ag–Au alloy on the surfaces of Ag nanocrystals should improve the stability of elemental Ag in an oxidative environment such as a solution containing an oxidant and/or halide ions.[30–32] We performed a series of experiments to evaluate the stability of the Ag–Au hollow nanocubes and nanoboxes by benchmarking against the Ag nanocubes. In a typical

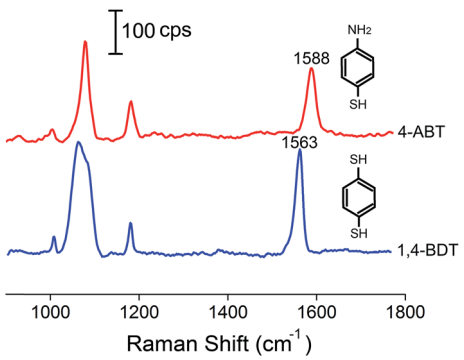

Fig. 4 SERS spectra of 1,4-BDT and ABT, respectively, adsorbed on the surfaces of Ag–Au hollow nanocubes. The samples were prepared using 1,4-BDT and ABT solutions of 10^{-9} M in concentration.

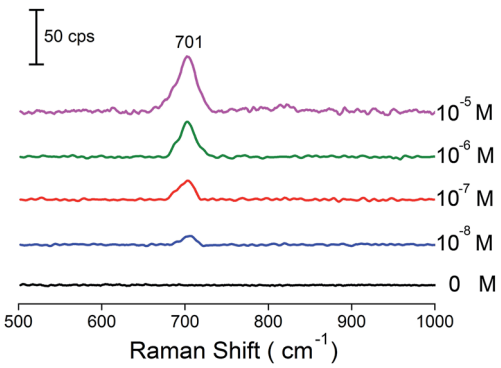

Fig. 5 SERS spectra of melamine adsorbed on the Ag–Au hollow nanocubes in which the samples were prepared from aqueous melamine solutions with different concentrations.

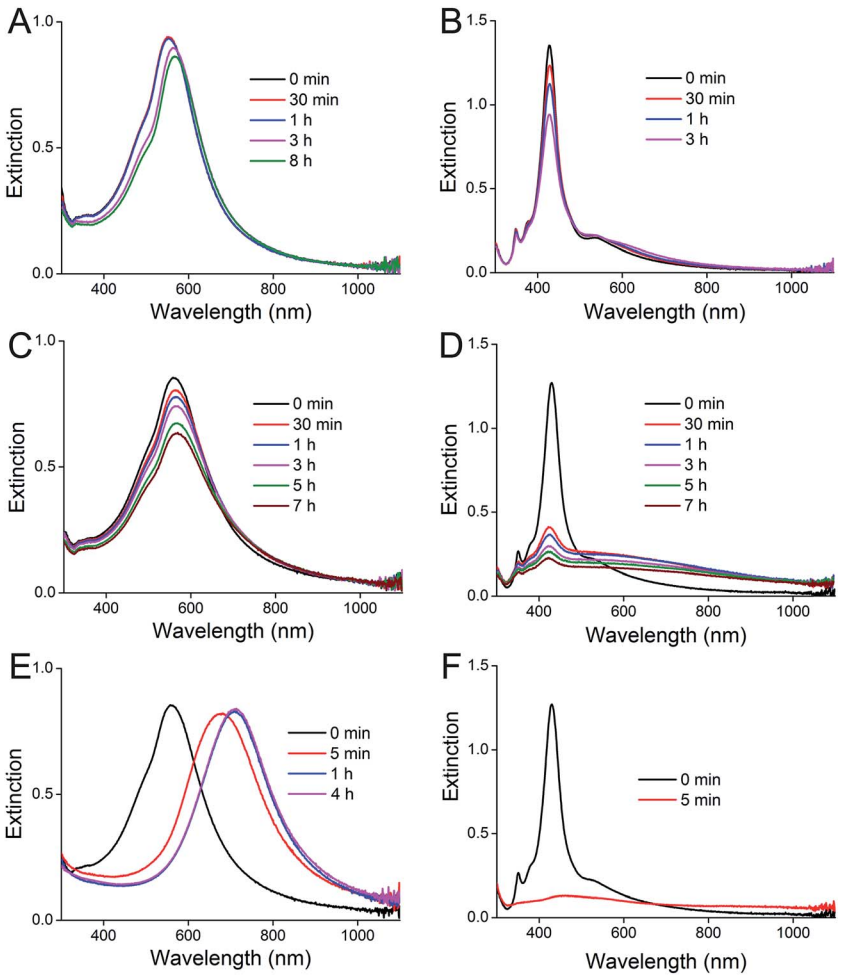

Fig. 6 UV-vis spectra of (A, C and E) Ag–Au hollow nanocubes and (B, D and F) Ag nanocubes in (A and B) phosphate buffer solution (10 mM), (C and D) NaCl solution (0.6 M), and (E and F)1% H_2O_2.

experiment, we dispersed the nanoparticles in a specifically formulated aqueous solution and recorded the UV-vis-NIR spectra as a function of time to monitor any possible changes in the morphology.

First, we investigated the effect of ionic species on the stability. The Ag–Au hollow nanocubes showed excellent stability in the phosphate buffer solution (PBS, 10 mM), with only a slight change to the LSPR peak position from 566 to 576 nm (Fig. 6A). The three LSPR peaks of Ag nanocubes were preserved in position, but there was a continuous decrease in intensity for the in-plane dipole peak located at 435 nm (Fig. 6B). Moreover, a shoulder peak appeared around 537 nm, indicating the formation of aggregates because of the decrease in colloidal stability. When we replaced the PBS solution with NaCl (0.6 M), the UV-vis-NIR spectra of the Ag–Au hollow nanocubes essentially remained unchanged for 7 h, but the intensity of the in-plane dipole peak decreased over time (Fig. 6C). In contrast, upon mixing of Ag nanocubes with aqueous NaCl for just 1 min, the LSPR peaks significantly changed with a dramatic drop in intensity for the in-plane dipole peak and a growth of a shoulder peak across the spectrum from the visible to the near-infrared (Fig. 6D). These results indicate that the Ag–Au hollow nanocubes have better stability against aggregation in a high ionic aqueous solution.

Next, we evaluated the chemical stability of the Ag–Au hollow nanocubes and Ag nanocubes in an oxidative environment such as 1% aqueous H_2O_2. Upon mixing with H_2O_2, the LSPR peak of the Ag–Au hollow nanocubes was quickly shifted from 566 to 678 nm within 5 min, and then to 699 nm and remained unaltered up to 4 h (Fig. 6E). These results indicate that, upon the removal of the residual pure Ag in the interior of each particle, the Ag–Au nanoboxes with a Ag–Au alloy shell of only 5.6 nm thickness exhibited excellent chemical stability. In contrast, the LSPR peak of the Ag nanocubes at 435 nm was completely diminished in intensity after only 5 min (Fig. 6F), which suggests poor stability for the original Ag nanocubes. The significant stability of Ag–Au hollow nanocubes and nanoboxes provides great potential for applications in the SERS detection and imaging of chemical and biological systems.

Conclusions

We have generated Ag–Au hollow nanocubes through the galvanic replacement reaction between Ag nanocubes and

$HAuCl_4$ in the presence of a reducing agent such as AA. The galvanic replacement reaction led to the release of Ag^+ ions from the interiors of Ag nanocubes, followed by the co-reduction of Ag^+ and $AuCl_4^-$ by AA to generate Ag and Au atoms for their deposition to form a continuous shell of Ag–Au alloy on the surface of each hollow nanocube. The Ag–Au hollow nanocubes were further transformed into nanoboxes upon removing the residual pure Ag with aqueous H_2O_2. We have systematically evaluated the SERS activities of the Ag–Au hollow nanocubes and nanoboxes by benchmarking against Ag nanocubes. We found that the Ag–Au hollow nanocubes, with contribution from the remaining pure Ag in the interiors, exhibited the strongest SERS activity, with remarkable detection sensitivity of 10^{-11} M and 10^{-8} M for 1,4-BDT and melamine, respectively. In addition, our results indicate that the Ag–Au nanoboxes with Ag–Au alloy shells of 5.6 nm thickness had a stronger SERS activity compared to the original Ag nanocubes. Both the Ag–Au hollow nanocubes and nanoboxes exhibited significantly improved chemical stability in a buffer, electrolyte, or aqueous H_2O_2 solution, making them good candidates for SERS detection in a variety of systems.

Acknowledgements

This work was supported by the start-up funds from Georgia Institute of Technology. Y.Y. was partially supported by the China Scholarship Council. Part of the work was performed in the Institute of Electronics and Nanotechnology (IEN) at the Georgia Institute of Technology, a member of the National Nanotechnology Infrastructure Network, which was partially supported by NSF (award no. ECS-0335765).

References

1 J. Kneipp, H. Kneipp and K. Kneipp, *Chem. Soc. Rev.*, 2008, **37**, 1052–1060.
2 E. Smith and G. Dent, *Modern Raman Spectroscopy, a Practical Approach*, Wiley-VCH, Weinheim, Germany, 2005.
3 S. Schlüucker, *Surface Enhanced Raman Spectroscopy. Analytical, Biophysical and Life Science Applications*, Wiley-VCH, Weinheim, Germany, 2011.
4 D. L. Jeanmaire and R. P. Van Duyne, *J. Electroanal. Chem.*, 1977, **84**, 1–20.
5 W. E. Doering and S. M. Nie, *Anal. Chem.*, 2003, **75**, 6171–6176.
6 M. Rycenga, C. M. Cobley, J. Zeng, W. Y. Li, C. H. Moran, Q. Zhang, D. Qin and Y. Xia, *Chem. Rev.*, 2011, **111**, 3669–3712.
7 P. Negri, K. T. Jacobs, O. O. Dada and Z. D. Schultz, *Anal. Chem.*, 2013, **85**, 10159–10166.
8 Y. J. Yang and G. W. Meng, *J. Appl. Phys.*, 2010, **107**, 0443151–0443155.
9 L. Guerrini, J. V. Garcia-Ramos, C. Domingo and S. Sanchez-Cortes, *Anal. Chem.*, 2009, **81**, 953–960.
10 A. K. Samal, L. Polavarapu, S. Rodal-Cedeira, L. M. Liz-Marzán, J. Pérez-Juste and I. Pastoriza-Santos, *Langmuir*, 2013, **29**, 15076–15082.
11 H. T. Ngo, H. N. Wang, A. M. Fales and T. Vo-Dinh, *Anal. Chem.*, 2013, **85**, 6378–6383.
12 S. W. Verbruggen, M. Keulemans, J. A. Martens and S. Lenaerts, *J. Phys. Chem. C*, 2013, **117**, 19142–19145.
13 L. B. Yang, G. Y. Chen, J. Wang, T. T. Wang, M. Q. Li and J. H. Liu, *J. Mater. Chem.*, 2009, **19**, 6849–6856.
14 K. Kim, K. L. Kim, J. Y. Choi, H. B. Lee and K. S. Shin, *J. Phys. Chem. C*, 2010, **114**, 3448–3453.
15 M. Fan, F. J. Lai, H. L. Chou, W. T. Lu, B. J. Hwang and A. G. Brolo, *Chem. Sci.*, 2013, **4**, 509–515.
16 C. B. Gao, Y. X. Hu, M. S. Wang, M. F. Chi and Y. D. Yin, *J. Am. Chem. Soc.*, 2014, **136**, 7474–7479.
17 M. Rycenga, X. H. Xia, C. H. Moran, F. Zhou, D. Qin, Z. Y. Li and Y. N. Xia, *Angew. Chem.*, 2011, **123**, 5587–5591.
18 S. E. Skrabalak, L. Au, X. D. Li and Y. N. Xia, *Nat. Protoc.*, 2007, **2**, 2182–2190.
19 M. Rycenga, K. K. Hou, C. M. Cobley, A. G. Schwartz, P. H. C. Camargo and Y. N. Xia, *Phys. Chem. Chem. Phys.*, 2009, **11**, 5903–5908.
20 R. G. Sanedrin, D. G. Georganopoulou, S. Park and C. A. Mirkin, *Adv. Mater.*, 2005, **17**, 1027–1031.
21 B. Rodríguez-González, A. Burrows, M. Watanabe, C. J. Kielyb and L. M. Liz Marzán, *J. Mater. Chem.*, 2005, **15**, 1755–1759.
22 M. M. Shahjamali, M. Bosman, S. W. Cao, X. Huang, S. Saadat, E. Martinsson, D. Aili, Y. Y. Tay, B. Liedberg, S. C. J. Loo, H. Zhang, F. Boey and C. Xue, *Adv. Funct. Mater.*, 2012, **22**, 849–854.
23 Y. Yang, Q. Zhang, Z. W. Fu and D. Qin, *ACS Appl. Mater. Interfaces*, 2014, **6**, 3750–3757.
24 X. H. Xia, J. Zeng, L. K. Oetjen, Q. Li and Y. X. Xia, *J. Am. Chem. Soc.*, 2012, **134**, 1793–1801.
25 Z. Guo, Z. Cheng, R. Li, L. Chen, H. Lv, B. Zhao and J. Choo, *Talanta*, 2014, **122**, 80–84.
26 X. F. Zhang, M. Q. Zou, X. H. Qi, F. Liu, X. H. Zhu and B. H. Zhao, *J. Raman Spectrosc.*, 2010, **41**, 1655–1660.
27 J. M. Li, W. F. Ma, C. Wei, L. J. You, J. Guo, J. Hu and C. C. Wang, *Langmuir*, 2011, **27**, 14539–14544.
28 A. Kim, S. J. Barcelo, R. S. Williams and Z. Y. Li, *Anal. Chem.*, 2012, **84**, 9303–9309.
29 B. Zhang, P. Xu, X. M. Xie, H. Wei, Z. P. Li, N. H. Mack, X. J. Han, H. X. Xu and H. L. Wang, *J. Mater. Chem.*, 2011, **21**, 2495–2501.
30 N. Murshid, I. Gourevich, N. Coombs and V. Kitaev, *Chem. Commun.*, 2013, **49**, 11355–11357.
31 C. Gao, Z. Lu, Y. Liu, Q. Zhang, M. Chi, Q. Cheng and Y. Yin, *Angew. Chem., Int. Ed.*, 2012, **51**, 5629–5633.
32 L. Shang, L. H. Jin, S. J. Guo, J. F. Zhai and S. J. Dong, *Langmuir*, 2010, **26**, 6713–6719.

